RMetS
Royal Meteorological Society

Adiabatic westward drift of Indian monsoon depressions

W. R. Boos,* J. V. Hurley and V. S. Murthy
Department of Geology and Geophysics, Yale University, New Haven, CT, USA

*Correspondence to: W. R. Boos, Yale University, PO Box 208109, New Haven, CT 06520-8109, USA.
E-mail: billboos@alum.mit.edu

A large fraction of the rain received by continental India is produced by cyclonic vortices with outer radii of about 1000 km that are contained within the larger scale South Asian monsoon flow. The more intense occurrences of these vortices are called monsoon depressions; these consist of bottom-heavy columns of relative vorticity that propagate to the northwest in time-mean low-level eastward flow. Previous studies have argued that this apparent upstream propagation is caused by dynamical lifting west of the vortex centre, with the resulting ascent producing vortex stretching that shifts the vortex to the west. Here, analysis of over 100 Indian monsoon depressions is used to show that low-level vortex stretching has a spatial structure inconsistent with the observed propagation and is balanced by other terms in the low-level vorticity budget. Instead, monsoon depressions are shown to consist of potential vorticity maxima that have peak amplitude in the middle troposphere and propagate westward by nonlinear, horizontal adiabatic advection (i.e. beta drift). The precipitating ascent in monsoon depressions makes a more minor contribution to the total storm motion and primarily acts to maintain the upright structure of the vortex. These results suggest a new view of Indian monsoon depressions as potential vorticity columns that propagate primarily by adiabatic dynamics.

Key Words: monsoon depressions; beta drift; monsoon low-pressure systems

Received 24 April 2014; Revised 30 July 2014; Accepted 1 September 2014; Published online in Wiley Online Library 13 November 2014

1. Introduction

Contained within the continental-scale, interhemispheric circulation of the South Asian summer monsoon are smaller scale cyclonic vortices called monsoon depressions. These storms have typical outer diameters of 2000 km, a cold core in the lower troposphere, moderate surface wind speeds and high rain rates (Godbole, 1977). They are a subset, when categorized by intensity, of a more general distribution of synoptic-scale cyclonic vortices called monsoon low-pressure systems; these systems collectively produce about half the total rainfall of the Indian summer monsoon (Sikka, 1977, 2006; Yoon and Chen, 2005). On average, 14 low-pressure systems are observed each year during June–September in the Indian monsoon region, with about half typically categorized as monsoon depressions.

Indian monsoon depressions (MDs) form most frequently over the Bay of Bengal and travel to the northwest over the Indian subcontinent (Sikka, 1977; Mooley and Shukla, 1987). This direction of propagation is remarkable because the time-mean low-level flow is eastward in monsoon regions; cyclonic winds peak in the lower troposphere in MDs, so one would expect the low-level mean flow to advect the vortex to the east. However, MDs exist in a region where the mean winds have westward vertical shear and it has been argued that the MD vortex interacts with this shear to produce ascent and vortex stretching to the west of the vorticity maximum. This interaction can be represented by an approximate form of the quasi-geostrophic omega equation (e.g. Sutcliffe, 1947; Trenberth, 1978):

$$L\omega \sim f_0 \frac{\partial \mathbf{u}_g}{\partial p} \cdot \nabla \left(2\zeta_g + f\right), \tag{1}$$

where ω is the vertical velocity in pressure coordinates, L is a three-dimensional Laplacian operator, f and f_0 are the Coriolis parameter and the mean Coriolis parameter, respectively, and $\mathbf{u}_g$ and ζ_g are the geostrophic wind and its relative vorticity, respectively. The right-hand side of Eq. (1) describes the dynamical generation of ascent downshear of a vorticity maximum. This ascent, in turn, produces low-level vortex stretching that has been argued to shift the MD vorticity maximum to the west.

This hypothesis for MD propagation dates back to Rao and Rajamani (1970), who showed that quasi-geostrophic lifting could produce ascent west of the peak relative vorticity in one MD observed in 1966. They argued that this ascent produces low-level vortex stretching that shifts the vorticity maximum to the west. Sanders (1984) similarly showed that the quasi-geostrophic omega equation applied to field programme observations of one MD in 1979 predicted ascent west of the vortex centre, with the resulting vortex stretching providing a decent estimate of the storm's westward motion. The occurrence of maximum precipitation and ascent to the west and southwest of the vortex centre has since been confirmed by multiple studies (Godbole, 1977; Saha and Chang, 1983; Sikka, 2006). Chen *et al.* (2005)

conducted a budget analysis of the horizontal stream function for 143 Indian monsoon low-pressure systems identified in reanalysis data and confirmed that vortex stretching in this ascending region provides a positive vorticity tendency west of the vortex centre.

All of these studies of vertical motion and vortex stretching in MDs either neglect interactions with moist convection (e.g. Rao and Rajamani, 1970) or treat it with a high degree of approximation. For example, Sanders (1984) obtained vertical velocities from the omega equation by assuming that the only effect of moist convection was to reduce the static stability to 1% of its typical dry value. Chen *et al.* (2005) did not diagnose vertical motion, but instead started with the vertical motion given by reanalyses and showed that it provided vortex stretching west of the vortex centre. Theory for the westward propagation of Indian MDs is thus missing a component that predicts the structure and amplitude of vertical motion around a sheared vortex in a precipitating atmosphere. While simply using a small effective static stability is compatible with some theories for moist convectively coupled flow (e.g. Emanuel *et al.*, 1994), it is not obvious that the first baroclinic, convective quasi-equilibrium framework upon which such effective static stabilities are based is appropriate for this particular application.

However, our motivation for re-examining the mechanism of MD propagation arises not from any obvious defect in the idea that quasi-geostrophic lifting produces movement of the vortex, but from inspection of the distribution of potential vorticity in several Indian MDs. Ertel's potential vorticity (EPV: Rossby, 1940; Ertel, 1942) is

$$q = \frac{1}{\rho}\boldsymbol{\eta} \cdot \nabla\theta, \tag{2}$$

where ρ is density, $\boldsymbol{\eta}$ is the absolute vorticity vector and θ is potential temperature. EPV is an appealing quantity because it is exactly conserved following the flow in the absence of diabatic heating and mechanical forcings such as friction and can be inverted to obtain the three-dimensional distribution of winds and temperatures (Hoskins *et al.*, 1985). A meridional profile through the centre of the MD examined by Sanders (1984) shows a vertical column of EPV, most of which is located in westward flow (Figure 1). Although MDs generally have relative vorticity that peaks in the lower troposphere, enhanced static stability in the mid-troposphere is associated with an EPV column with maximum amplitude near 450 hPa. This EPV maximum is located above the climatological mean eastward flow (i.e. above the magenta line in the online version of Figure 1) in a region where the total flow is westward with a speed exceeding 5 m s^{-1}. If this EPV maximum is not modified materially by diabatic heating or mechanical forcings, one would expect it simply to be advected to the west. At the same time, the bottom part of the EPV column would be advected to the east by the low-level flow, tilting the EPV column.

Numerous questions arise from examination of this EPV structure. For example, is vortex movement dominated by adiabatic EPV advection or by diabatically induced EPV tendencies? Are diabatic EPV tendencies needed to prevent the vortex from being tilted by shear, or is the upright structure maintained by adiabatic dynamics (e.g. the tropical cyclone dynamics described by Reasor and Montgomery, 2001; Reasor *et al.*, 2004)? Given that there are large differences between the climatological mean zonal flow and the instantaneous flow, does nonlinear advection dominate the advective tendencies of EPV, rather than linear advection by the mean flow? Or do intraseasonal variations in zonal wind still allow one to think of the vortex as being advected by a local time-mean flow? Does Figure 1 represent the EPV structure of a typical MD and its position relative to the line of zero zonal wind? This article seeks to answer these and other questions related to the propagation of Indian MDs. Issues related to the genesis and subsequent growth of these storms will be addressed in a separate work.

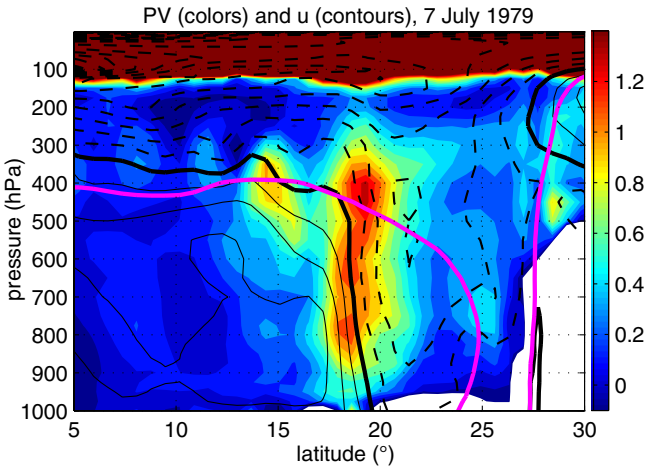

Figure 1. Shading/colours show Ertel's potential vorticity (EPV) as represented in ERA-Interim, for 7 July 1979 at 0600 UTC and 87°E, in PV units (PVU; 1 PVU = 10^{-6} K m^2 kg^{-1} s^{-1}). Black contours show the zonal wind at the same time, with negative (westward) values dashed, a contour interval of 5 m s^{-1} and the thick black line representing the zero contour. The grey line (magenta in online) is the zero contour of zonal wind from a daily climatology (1979–2012) for 7 July. Regions below topography are in shown in white.

The dynamics of precipitating, synoptic-scale vortices propagating in the downshear direction have been explored in much greater detail in the context of midlatitude vortices in eastward shear. Raymond and Jiang (1990) proposed that precipitation occurring in the ascent region downshear of a mesoscale convective vortex will produce a source of EPV in the lower troposphere that maintains the initial vortex. Snyder and Lindzen (1991) showed that a particular moisture-convergence closure for precipitation can destabilize waves that are structurally similar to dry baroclinic waves but are produced instead by the EPV tendencies associated with moist diabatic heating. Subsequent studies using idealized nonlinear moist models have shown that an isolated 'diabatic Rossby vortex' will propagate downshear, because low-level diabatic EPV generation in the region of quasi-geostrophic lifting plays a role analogous to that of meridional EPV advection in a traditional Rossby wave (Parker and Thorpe, 1995; Montgomery and Farrell, 1991, 1992; Moore and Montgomery, 2004, 2005). It is unclear how the dynamics will be altered by the westward shear and the slightly lower latitude setting that characterizes MDs. Indeed, the possible connection between an MD and a diabatic Rossby vortex seems entirely unexplored, even though the diabatic Rossby vortex propagation mechanism is nearly identical to that proposed decades earlier for MDs (e.g. compare Rao and Rajamani, 1970; Raymond and Jiang, 1990).

The effects of both eastward and westward vertical shear on columns of vorticity in the Tropics have been well explored in the context of tropical cyclones (for reviews see Wang *et al.*, 1999; Chan, 2005). For example, Jones (1995) and Wang and Holland (1996) found that ascent initially occurs downshear of a dry, adiabatic vortex as the vortex undergoes tilting by the shear. This generates the temperature anomalies needed to keep the vortex in balance; then, in a balanced state, the vertical motion dipole becomes orthogonal to the shear vector, with ascent occurring to the right of an observer looking in the downshear direction. However, the relevance of this literature to MDs is unclear because of the substantially larger size, lower wind speeds and distinct thermal core structure of MDs.

The goal of this study is to improve understanding of the propagation of Indian MDs, but the results may be relevant to disturbances in other regions. Monsoon depressions also form in the Australian monsoon and in the West Pacific, although they have been studied less in those regions. Nevertheless, Davidson and Holland (1987) concluded that two Australian MDs examined in a case study had structures similar to those of Indian MDs. Australian MDs are also part of a broader distribution of synoptic low-pressure systems, 10–15 of which occur each month, on

average, in the Australian summer monsoon (Berry *et al.*, 2012). West Pacific MDs are similarly abundant, but it is unclear whether they are dynamically similar to Indian and Australian depressions, despite recent examinations of West Pacific storms (e.g. Beattie and Elsberry, 2012, 2013). A comparative study of MD structure in different regions is presented in a separate work (Hurley and Boos, 2014).

Finally, we note that several previous authors have associated MDs with the cyclonic part of Rossby waves. Goswami (1987) argued that Indian MDs propagate westward because frictional convergence in a Rossby gyre west of a tropical heat source produces ascent and vortex stretching to the west of the original heat source. Sobel and Horinouchi (2000) argued that latent heating associated with off-equatorial mesoscale convective systems could excite short Rossby waves with characteristics similar to those of MDs and other synoptic-scale tropical disturbances. However, these arguments require the convective maximum to lie east of the vorticity maximum, while in observations the convective maximum lies to the westsouthwest of the vortex centre (e.g. Godbole, 1977). Equatorial Rossby waves altered by the monsoonal mean state are known to produce large wind and rain variability over the Indian monsoon region, but this variability has a spectral peak with an approximate two-week period that is clearly separated from synoptic-scale variability (Chatterjee and Goswami, 2004). We therefore conclude that MDs are not simply the cyclonic part of equatorial Rossby waves. Nevertheless, we admit that the present study takes a vortex-centred view of MDs and does not perform any spectral filtering, so it is likely that some of the MDs examined here are associated with equatorial waves or other intraseasonal disturbances.

The next section of this article details the data and methodology used here. We then present some general characteristics of MD propagation and reveal flaws in the theory of low-level, quasi-geostrophic lifting that has previously been invoked to explain propagation. The distribution and evolution of EPV in MDs is then presented to support a new hypothesis for the mechanism of propagation. We conclude with a discussion of the implications and issues meriting further exploration.

2. Data and methods

Most results presented here are obtained from analysis of an ensemble of Indian MDs identified in ERA-Interim, the most recent reanalysis of the European Centre for Medium-Range Weather Forecasts (ECMWF: Dee *et al.*, 2011). We use the gridded, pressure-level ERA-Interim product at a horizontal resolution of roughly $0.7^\circ \times 0.7^\circ$ and a temporal resolution of 6 h. We also use version 7 of the 3B42 daily estimate of precipitation from the Tropical Rainfall Measuring Mission (TRMM).

Monsoon depressions are identified using an automated algorithm that selects tracks of low-level relative vorticity maxima having surface wind speeds and sea-level pressure anomalies consistent with the India Meteorological Department (IMD) definition of an MD (e.g. Mooley and Shukla, 1987; Sikka, 2006; Ajayamohan *et al.*, 2010). The detailed methodology and a validation of its performance are presented in a companion article (Hurley and Boos, 2014) and only a summary is given here. Tracks of 850 hPa relative vorticity maxima are obtained using an automated, objective algorithm described by Hodges (1995, 1998). The 850 hPa level was chosen because it lies above most of the planetary boundary layer but is still at low levels where the vorticity of MDs peaks. Several previous studies that tracked Indian MDs also focused on the 850 hPa level (Sanders, 1984; Chen and Weng, 1999; Yoon and Chen, 2005). Only vortices with an 850 hPa relative vorticity maximum that exceeds $1 \times 10^{-5}\ \mathrm{s}^{-1}$ are retained; at the ERA-Interim resolution this is a lax criterion that includes many vortices much weaker than MDs. For this reason, the vortices are also required to have a sea-level pressure anomaly, relative to a 21-day running mean, with an amplitude of 4–10 hPa and a surface wind speed between 8.5 and 13.5 $\mathrm{m\,s}^{-1}$. These pressure and wind criteria must be satisfied within 500 km of the 850 hPa vorticity maximum and must occur concurrently during at least one 6 h period along the vortex track. Those vortices that simultaneously achieve more or less intense sea-level pressure anomalies and surface wind speeds are categorized as deep depressions and lows, respectively, and are not included in our ensemble of MDs. While we do not expect qualitative differences between the weakest vortices categorized as deep depressions and those categorized as depressions, we want to avoid including storms strong enough to achieve tropical cyclone intensity with warm cores and coherent eyewalls. In the broad Indian monsoon domain of 50–105°E, 0–30°N during June–September 1979–2012, there are 171 vortex tracks in ERA-Interim that satisfy these criteria for classification as MDs. This constitutes our set of MDs, although all composites presented here use only the subset of 117 storms with genesis points in the central domain of 75–95°E, 10–27°N (rectangular box in Figure 2(a)) because of its more regular direction of propagation. Within that smaller domain, there are 249 monsoon lows and only eight deep depressions, none of which are included in our analysis.

Composite means are created by averaging variables of interest relative to the storm centre, which is defined as the location of the 850 hPa relative vorticity feature as identified by the tracking algorithm. Six-hourly fields of data are first averaged over times within individual storms and then a composite storm structure is produced by averaging over all storms. Each storm thus has the same weight in the composite mean. All composites shown here use only the middle third of a storm's lifetime, to avoid the early and late stages of the life cycle when storm intensity is weaker and when tendencies associated with storm growth or decay would complicate the analysis of tendencies associated with propagation. Averages are always taken over an integral number of 24 h periods to avoid sampling the diurnal cycle unevenly. The average lifetime of Indian MDs in our dataset is 7.5 days, so eight six-hourly fields are used on average in the composite for a storm, with 117 storms then averaged to create the ensemble composite mean. The standard deviation of storm lifetime is 3.8 days. Although the ERA-Interim dataset provides values for variables at pressures larger than that of the surface, those extrapolated values are omitted from any composite means taken here. For this reason, many vertical sections shown here terminate at a lower boundary of 950 hPa.

A case study of one storm occurring in September 2008 uses the ECMWF Year of Tropical Convection (YOTC) analysis (Moncrieff *et al.*, 2012), which is available for May 2008–April 2010. This analysis uses a spectral *T*799 atmospheric model with 97 vertical levels and we use gridded output available every 6 h at a horizontal resolution of $1^\circ \times 1^\circ$. The ECMWF–YOTC dataset provides tendencies associated with model parametrizations, which are used here to calculate the diabatic EPV tendencies for one MD. The September 2008 storm was chosen because it was one of the few MDs occurring during the period of the YOTC analysis that exhibited classic northwest propagation.

3. Results I: flaws in the idea of low-level quasi-geostrophic control

3.1. General propagation characteristics

The distribution of genesis locations for Indian MDs was obtained by calculating the number of tracks originating at each horizontal location in the ERA-Interim dataset, then smoothing with a Gaussian kernel having an isotropic standard deviation (i.e. horizontal length-scale) of 2°. The result shows that most MDs form over the northern Bay of Bengal, but some also form over the eastern Arabian Sea and parts of continental India (Figure 2(a)). This genesis distribution is consistent with that known from previous studies (e.g. Krishnamurti *et al.*, 1977; Saha *et al.*, 1981; Krishnamurthy and Ajayamohan, 2010). An average of five MDs form each June–September season over the domain shown in Figure 2(a).

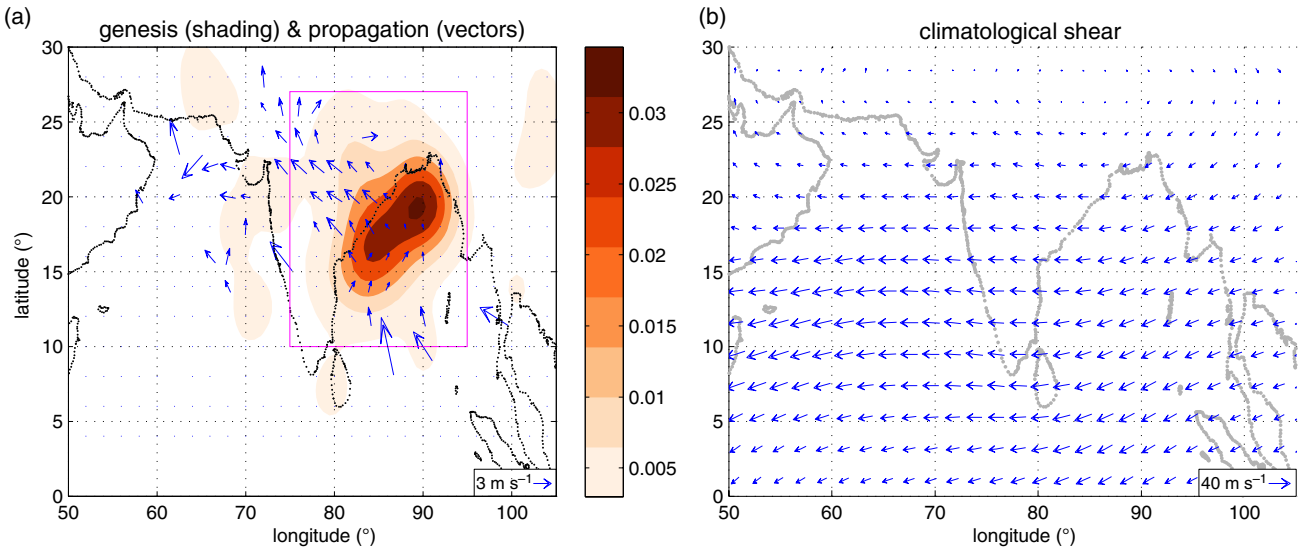

Figure 2. (a) Shading/colours show the number of genesis points per square degree (roughly 12 000 km^2) per summer season (June–September), after smoothing with a Gaussian filter. Vectors show the average propagation speed of MDs and are coarsened to a 2° × 2° grid for clarity; vectors are shown only if the mean zonal or meridional propagation speed at each grid point is statistically significant at the 1% level by a two-tailed *t*-test. (b) June–September climatological mean vertical shear vector, defined as the 200–850 hPa horizontal wind.

The propagation of MDs was characterized by averaging the vector motion of all storm centres passing through each horizontal location. Vectors are shown only if either the *x*- or *y*-component of the mean propagation velocity is significantly different from zero at the 1% level by a two-tailed *t*-test. For depressions that form over the Bay of Bengal, which constitute most of the MD population, propagation is to the northwest at speeds of 2–3 m s^{-1}. This is slower than the 5° longitude day^{-1} (i.e. 6 m s^{-1}) sometimes cited as a propagation speed (e.g. Krishnamurti *et al.*, 1975; Yoon and Huang, 2012), but is consistent with the speeds obtained by Sanders (1984) in his case study of one MD in 1979. The propagation direction and speed vary with location, with MDs that reach northern India turning northward and then eastward. Although much fewer in number, MDs over the southern Bay of Bengal travel northward at faster speeds near 5 m s^{-1} and MDs over the eastern Arabian Sea exhibit more spatial variability in their direction of propagation.

Given that the vector vertical wind shear (defined as the 200 hPa wind minus the 850 hPa wind) exhibits a smaller spatial variability and points to the northwest almost nowhere in the domain (Figure 2(b)), the distribution of propagation vectors seems inconsistent with the idea that MD propagation is primarily controlled by quasi-geostrophic ascent downshear of the vortex centre. However, time or vertical variations in the shear vector could allow for different directions of propagation than might be inferred from this seasonal mean 200–850 hPa shear. Alternatively, other terms in the vorticity budget could produce storm motion substantially different from that due to downshear stretching alone; this would necessitate a different interpretation of the propagation mechanism but might still be thought of as low-level, quasi-geostrophic control of storm motion. To resolve these and related issues, we next examine in detail the dynamics of the low-level vorticity maximum.

3.2. *The relevance of low-level vortex stretching*

The composite mean Indian MD consists of a column of positive relative vorticity that has peak amplitude in the lower troposphere and is contained almost entirely within the layer of climatological mean eastward wind (Figure 3). The zonal wind shown in Figure 3 is a storm-centred climatology obtained by sampling a daily zonal wind climatology centred on each track position and then, as is standard here, averaging first over all times in the middle third of each storm's track and then over all storms. This composite confirms that the observed

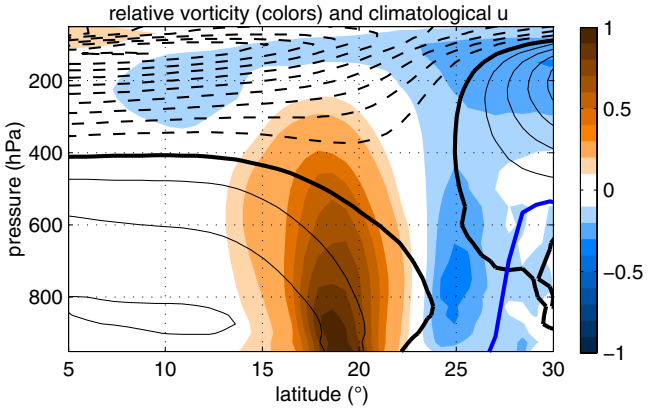

Figure 3. The composite mean vertical component of relative vorticity (colour shading, interval 0.1 × 10^{-4} s^{-1}) and climatological mean zonal wind (contours, interval 3 m s^{-1}, dashed negative and zero contour in bold). The climatological wind is a composite mean climatology relative to the storm centre, as described in the text.

northwestward propagation is upstream of the climatological mean flow in which the relative vorticity structure is embedded.

Multiple studies have argued that quasi-geostrophic lifting downshear (i.e. west) of the low-level vortex centre produces vortex stretching that shifts the vortex to the west, as discussed in the Introduction. However, the question of whether the asymmetric distribution of ω about the vortex centre can be explained by quasi-geostrophic lifting has been examined only in individual case studies (e.g. Rao and Rajamani, 1970; Daggupaty and Sikka, 1977; Saha and Chang, 1983; Sanders, 1984). Here we examine the dynamics responsible for the horizontal distribution of ω by using the full quasi-geostrophic omega equation,

$$\left(\sigma\nabla^2 + f_0^2\frac{\partial^2}{\partial p^2}\right)\omega = -2\nabla\cdot\mathbf{Q} - \frac{R}{p}\beta\frac{\partial T}{\partial x}, \qquad (3)$$

where $\sigma = \rho^{-1}\partial_p \ln\theta$, β is the meridional gradient of the Coriolis parameter and R is the gas constant. This is the so-called Q-vector form given by Hoskins *et al.* (1978) and Bluestein (1992) and includes terms associated with deformation and the gradient of the Coriolis parameter that were omitted in Eq. (1). Instead of computing $\mathbf{Q}$ and then its divergence, we use an approximate form of $\nabla\cdot\mathbf{Q}$ in which the irrotational part of the horizontal

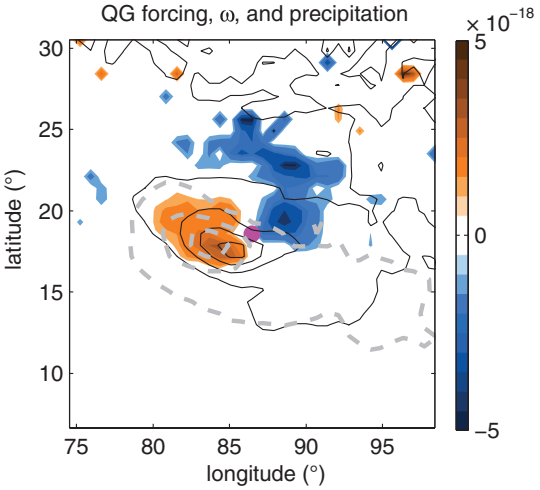

Figure 4. Shading shows the composite mean dynamical forcing for ascent (orange) and subsidence (blue) represented by the right-hand side of the quasi-geostrophic omega equation at 775 hPa, with a contour interval of 5×10^{-19} Pa^{-1} s^{-3}. Black solid contours show the composite mean vertical velocity in pressure coordinates at 775 hPa, with negative values (i.e. upward motion) represented by solid lines and a contour interval of 7×10^{-2} Pa s^{-1}. Grey dashed contours show the composite mean TRMM precipitation (for 1998–2012), with a contour interval of 15 mm day^{-1}. The magenta dot marks the location of the storm centre.

wind is neglected:

$$\frac{p}{R}\nabla\cdot\mathbf{Q} \simeq \frac{\partial T}{\partial x}\frac{\partial \zeta}{\partial y} - \frac{\partial T}{\partial y}\frac{\partial \zeta}{\partial x} - \frac{\partial^2 T}{\partial x \partial y}\left(\frac{\partial^2 \psi}{\partial x^2} - \frac{\partial^2 \psi}{\partial y^2}\right) + \frac{\partial^2 \psi}{\partial x \partial y}\left(\frac{\partial^2 T}{\partial x^2} - \frac{\partial^2 T}{\partial y^2}\right). \quad (4)$$

Here ζ is the vertical component of relative vorticity, ψ is the stream function of the horizontal wind, T is temperature and all horizontal derivatives are computed in spherical coordinates. This form of $\nabla \cdot \mathbf{Q}$ was used by Kiladis *et al.* (2006) in a study of African easterly waves (also see the discussion in Davies-Jones, 1991). The right-hand side of Eq. (3) was computed for every six-hourly period along the middle third of each MD track and then the composite mean was taken (i.e. we did not compute $\nabla \cdot \mathbf{Q}$ from composite mean values of T, ζ and ψ).

The dynamical forcing for vertical motion represented by the right-hand side of Eq. (3) has a horizontal distribution that qualitatively matches the distribution of ω (Figure 4). The pressure level of 775 hPa was chosen for this analysis because it is near the level at which ascent has its peak amplitude in a mature Indian MD (see below); ω was obtained from ERA-Interim. The ascent peaks southwest of the vortex centre in roughly the same location as the maximum values of the forcing represented by the right-hand side of (3). Equally strong forcing for subsidence exists to the northeast of the vortex centre and, although total subsidence is not seen there, anomalous subsidence relative to a daily climatology is observed with some spatial offset from this forcing (not shown). We do not invert the forcing to obtain a predicted value for ω because, as noted in the Introduction, moist convection is expected to interact with any dynamical lifting to alter ω greatly and it is unclear how to modify Eq. (3) to represent this interaction. Nevertheless, this result shows that peak ascent occurs southwest of the low-level vorticity maximum and confirms that the horizontal structure of ω can be qualitatively explained by quasi-geostrophic lifting. The maximum composite-mean TRMM precipitation (shown by the dashed grey contours in Figure 4) also occurs southwest of the low-level vorticity maximum, as expected given the location of the ascent maximum. Since this precipitation estimate is derived from satellite data, it shows that these MDs and their spatial structure of ascent are not artifacts of the numerical model used to create the ERA-Interim product.

To determine how this distribution of ascent alters storm vorticity, we compute all terms in the inviscid vorticity budget:

$$\frac{\partial \zeta}{\partial t} = -\eta\nabla\cdot\mathbf{u}_\mathrm{h} - \mathbf{u}_\mathrm{h}\cdot\nabla\eta - \omega\frac{\partial \zeta}{\partial p} - \frac{\partial \omega}{\partial x}\frac{\partial v}{\partial p} + \frac{\partial \omega}{\partial y}\frac{\partial u}{\partial p}, \quad (5)$$

where $\mathbf{u}_\mathrm{h}$ is the horizontal vector wind, η is the local vertical component of the absolute vorticity vector and other symbols have their usual meteorological meanings. This is the exact vorticity budget, not the quasi-geostrophic form, and we present the composite mean of individual terms in this budget, not approximate tendencies computed from composite mean winds. The first term on the right-hand side of Eq. (5) represents the vortex stretching previously argued to be responsible for shifting the vortex to the west. At 850 hPa, which is the level studied by Chen *et al.* (2005) in their analysis of Indian MD propagation, the composite mean vortex stretching produces a positive vorticity tendency southwest of the vortex centre (Figure 5(b)). This vortex stretching is very large compared with the Eulerian tendency (i.e. the observed rate of change of relative vorticity, Figure 5(a); note the change in colour scale) and has a maximum that is southwest, rather than northwest, of the vortex centre. A large part of the vortex stretching is balanced by horizontal vorticity advection (Figure 5(c)), with the latter having a dipole structure that points to the northeast.

Cancellation between vorticity stretching and advection is common and the net effect of the two can be more easily interpreted using the flux form of the vorticity equation as written by Haynes and McIntyre (1987) in pressure coordinates:

$$\frac{\partial \zeta}{\partial t} = -\nabla\cdot(\eta\mathbf{u}_\mathrm{h}) + \nabla\cdot\left(\omega\hat{\mathbf{k}}\times\frac{\partial \mathbf{u}_\mathrm{h}}{\partial p}\right). \quad (6)$$

The first term on the right-hand side of Eq. (6) represents the combined effects of stretching and horizontal advection and has been called the divergence of the advective flux of vorticity. The second term on the right-hand side represents the combined effects of vertical advection of ζ and tilting of horizontal components of the vorticity vector and has the form of the divergence of a non-advective flux. The advective flux divergence has a much smaller peak amplitude than either the stretching or advective terms, consistent with cancellation between those latter terms (Figure 5(d); again note the change in colour scale). Although its maximum lies southwest of the vortex centre, it has a secondary maximum northeast of the vortex centre that results from horizontal vorticity advection. The non-advective flux divergence is small compared with the advective flux divergence. The net right-hand side of Eq. (6) is thus nearly equal to the advective flux divergence, but provides a poor match to the observed tendency. We suggest that this disagreement results from the neglected mechanical forcing, which at 850 hPa could be substantial because of friction and momentum transport by boundary-layer turbulence. We tried adding several different simple representations of boundary-layer drag, but none of these was large enough to balance the apparent residual in the inviscid vorticity budget. However, it is possible that cumulus momentum transport would provide a large negative vorticity tendency in the heavily precipitating region southwest of the vortex centre, exactly where the budget residual is largest. It is also possible that horizontal gradients in surface roughness and orography are important, as both are highly variable in this region, or that ERA-Interim analysis tendencies play a large role. Altogether, this indicates that it is difficult to infer a mechanism of MD propagation from the 850 hPa vorticity budget unless such details are known.

At the higher level of 700 hPa, where mechanical damping is typically less important, the composite mean of the right-hand side of Eq. (6) is indeed a closer match to the observed tendency (Figure 6(a) and (f)). Although the right-hand side of Eq. (6) has a negative tendency that is too weak southeast of the vortex centre

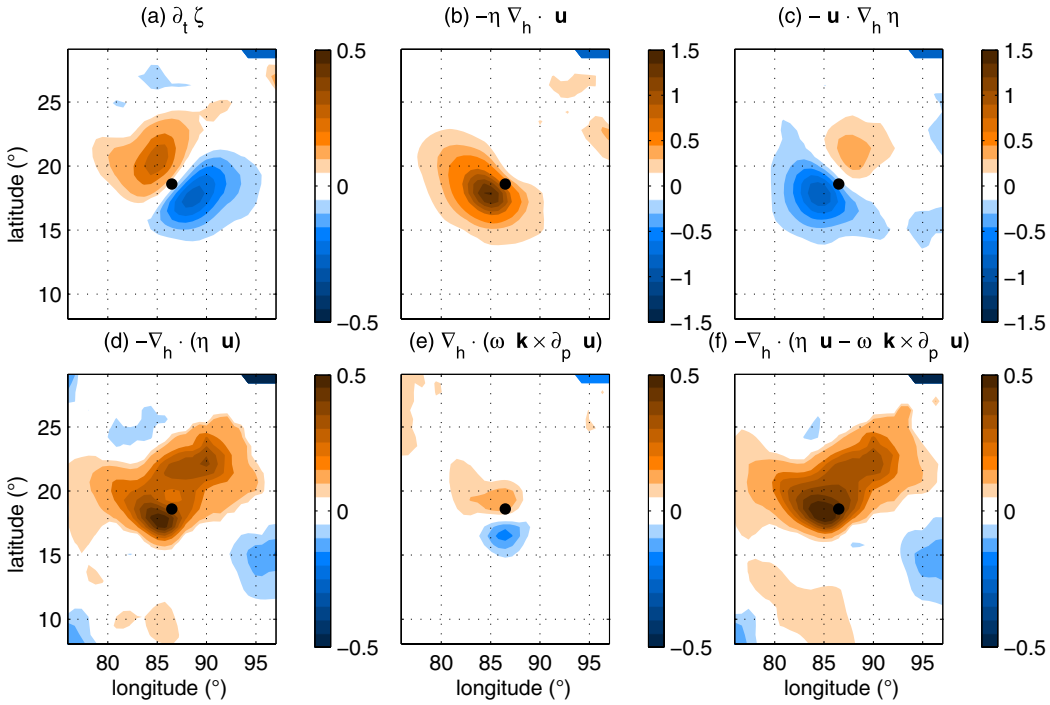

Figure 5. Select terms in the composite mean vorticity budget at 850 hPa. (a) The Eulerian rate of change of relative vorticity, (b) vortex stretching, (c) horizontal vorticity advection, (d) the convergence of the advective flux of vorticity (the sum of (b) and (c)), (e) the convergence of the non-advective flux of vorticity (the sum of vertical advection and tilting) and (f) the sum of all individual terms in the vorticity budget (orange and blue in online represents positive and negative tendencies, in units of 10^{-4} s^{-1} day^{-1}). Note the larger colour scale used in (b) and (c). The black dot marks the location of the storm centre. Only values significant at the 5% level by a two-tailed t-test are shown.

and also has a northward bias in the orientation of its dipole structure, it represents propagation to the north-northwest at a rate similar to that observed. At 700 hPa, vortex stretching southwest of the vortex centre is again nearly balanced by horizontal advection, with both terms having weaker tendencies than at 850 hPa. This indicates that horizontal advection by the vertically sheared mean flow tilts the vortex column and vortex stretching by downshear ascent acts primarily to oppose this tilting and maintain the upright structure of the column. None of the individual terms in either form of the vorticity budget can be viewed as dominating the net tendency. There is substantial cancellation between the advective flux divergence and the non-advective flux divergence. The positive tendency northwest of the centre that is needed to produce the observed propagation comes from a combination of advective and non-advective flux, with some uncertainty due to the budget residual. Convective momentum transport, boundary-layer processes or analysis tendencies may play a role in this residual, although these are not provided in the ERA-Interim output and there is no obvious way to obtain an estimate of their effects.

In summary, previous studies have relied on the idea of low-level vortex stretching to explain why Indian MDs propagate to the west against the time-mean low-level flow. We confirmed that quasi-geostrophic lifting southwest of the vortex centre can qualitatively explain the horizontal distribution of ascent. However, the vortex stretching produced by this ascent serves primarily to maintain the upright structure of the vortex, which would otherwise be tilted by the vertically sheared flow. The vortex stretching does not have a spatial structure that can explain the observed propagation. Detailed examination of the vorticity budget reveals a high degree of cancellation between vortex stretching, tilting and advection, making it difficult to attribute the northwest propagation to any single process.

3.3. *Invalidity of the quasi-geostrophic approximation*

Multiple previous studies have relied on quasi-geostrophic models to understand the dynamics of Indian MDs (e.g. Rao and Rajamani, 1970; Keshavamurty *et al.*, 1978; Sanders, 1984). However, the quasi-geostrophic approximation requires a Rossby number much less than unity and this requirement does not hold for MDs. In particular, the July 1979 depression shown in Figure 1 has zonal wind changing by 15 m s^{-1} over a distance of about 200 km and thus has a Rossby number (U/fL) of about 1.8. If one instead defines the Rossby number as the ratio of the vertical component of relative vorticity to the Coriolis parameter, one obtains $\zeta/f \backsim 2$ for the composite mean MD (e.g. Figure 3).

The quasi-geostrophic system has been known to help in understanding dynamical phenomena even when it is not strictly valid, but we show here that it provides a distorted view of Indian MDs. Davis (1992) and Hakim *et al.* (1996) demonstrated that quasi-geostrophy may provide useful insight into the dynamics of disturbances with Rossby number greater than unity if the analogue of PV in the quasi-geostrophic framework, the pseudo-potential vorticity q_p (also referred to as the QGPV), closely resembles the EPV. As defined by Charney and Stern (1962),

$$q_p = \frac{1}{f_0}\nabla^2\phi' + f + f_0\frac{\partial}{\partial p}\left(\frac{1}{\sigma}\frac{\partial \phi'}{\partial p}\right), \tag{7}$$

where the geopotential anomaly ϕ' is defined as the deviation from the annual mean geopotential height averaged over the entire Tropics (30°S–30°N), and the static stability σ is also a pressure-dependent tropical mean quantity. For the composite mean MD, q_p not surprisingly has a structure similar to that of the relative vorticity, peaking in the lower troposphere and decaying strongly with height above 700 hPa (Figure 7). One might expect this column of q_p to be tilted by the vertically sheared mean flow and advected to the east, since it lies almost entirely within the low-level eastward flow. Diabatic and mechanical forcings must provide the q_p tendencies needed to maintain an upright structure and produce a northwestward propagation. Upward motion (black contours in Figure 7) is greatest west of the vortex centre and the abundant precipitation known to occur in the ascent region of MDs might provide the mid-tropospheric diabatic heating needed to shift the q_p column to the west.

However, the q_p distribution differs greatly from the EPV distribution. The composite mean EPV has a maximum centred at 500 hPa and a weaker secondary maximum at about 700 hPa

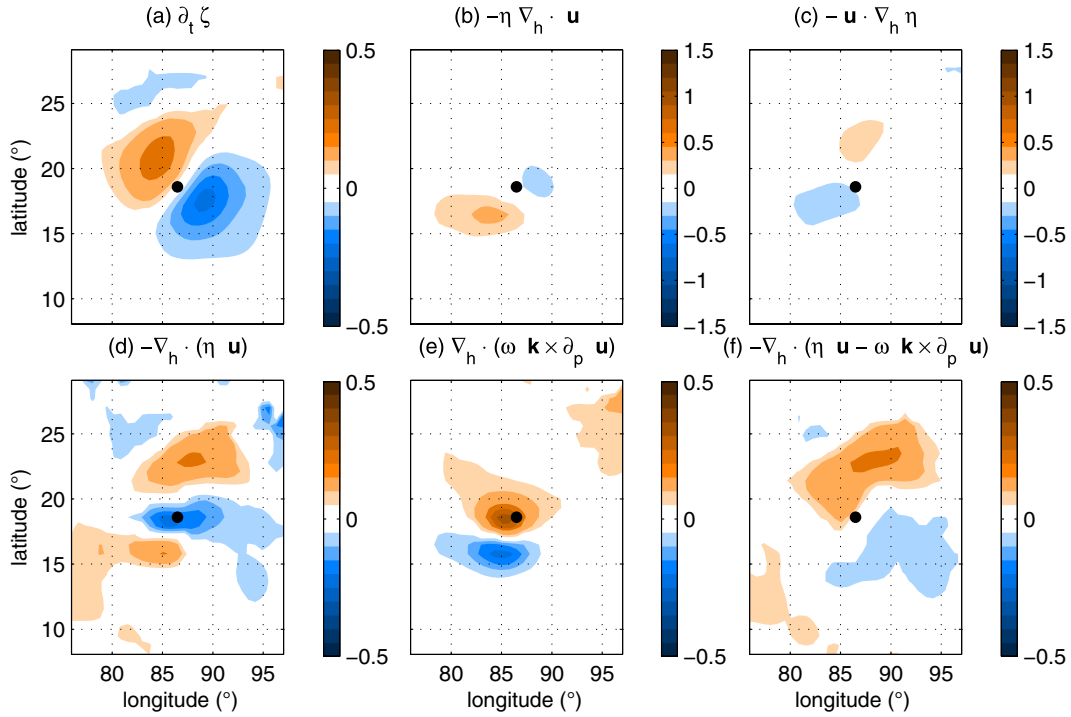

Figure 6. As in Figure 5, but at 700 hPa.

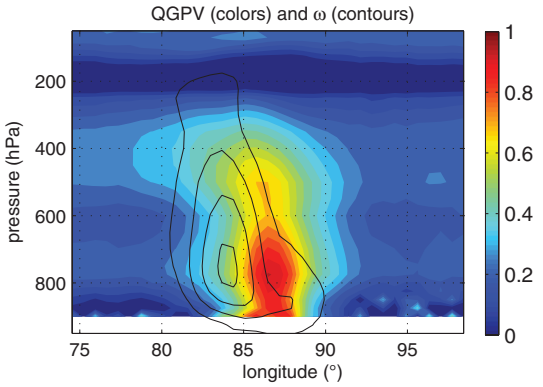

Figure 7. The quasi-geostrophic pseudopotential vorticity, q_p (shading/colours, in PVU) and the vertical velocity anomaly, relative to a daily climatology (contours: solid contours show upward values, interval 4×10^{-2} Pa s^{-1}). The values of q_p are scaled by $-g\partial\theta/\partial p$ evaluated at 900 hPa. Values of q_p below 900 hPa are not shown because of the vertical differencing performed in computing this quantity.

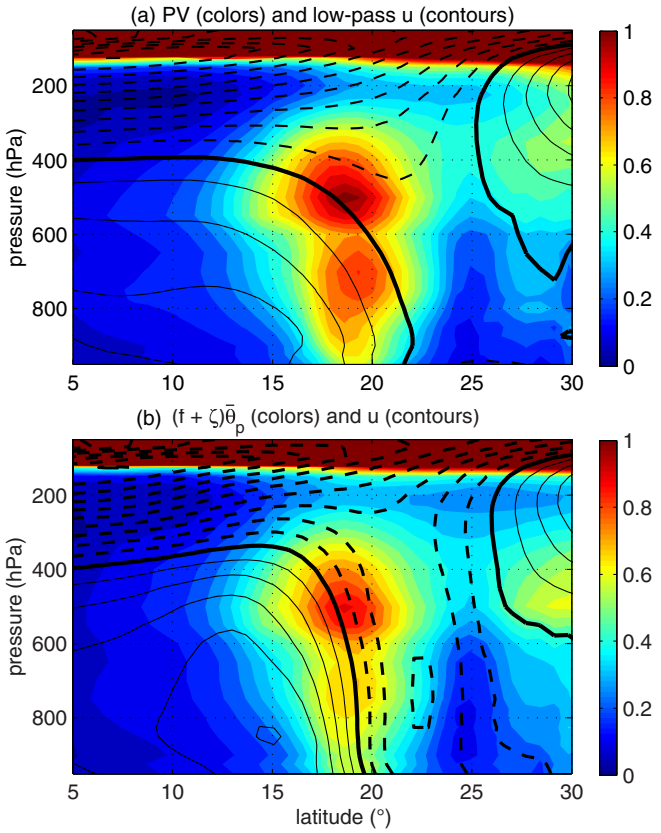

Figure 8. (a) Composite mean Ertel's potential vorticity (EPV, shading/colours, units of PVU) and 21 day smoothed zonal wind (contours). (b) An approximate form of EPV obtained by multiplying the composite mean absolute vorticity by the climatological mean static stability (shading/colours), overlaid with the total zonal wind (contours). In both panels, zonal wind contours are dashed for negative values, with the zero contour in bold and an interval of 3 m s^{-1}.

(Figure 8(a)). Although the vertical structure of EPV in the single MD shown in Figure 1 is less bimodal than the composite mean vertical structure, that particular case still consists of a vertical column of EPV with maximum amplitude in the middle troposphere. Inspection of other MDs shows that many individual storms do have bimodal EPV distributions. The mid-tropospheric EPV maximum exists because the mid-troposphere is more statically stable than the lower troposphere in the climatological mean over the Bay of Bengal. In other words, we find that the EPV field is decently approximated by

$$q \simeq -g(f + [\zeta])\frac{\partial \overline{\theta}}{\partial p}, \tag{8}$$

where an overbar denotes a June–September climatological mean over the central Bay of Bengal (87°E, 19°N) and $[\zeta]$ is the composite mean vertical component of the relative vorticity (Figure 8(b)). This approximate form of EPV reproduces the mid-tropospheric EPV maximum because $\partial_p \overline{\theta}$ has a vertical gradient and is multiplied by $[\zeta]$, which has horizontal gradients. Thus, although MDs have a warm-over-cold core structure (e.g. Godbole, 1977) that enhances the mid-tropospheric static stability precisely where ζ is large, these horizontal variations in static stability are not the primary cause of the mid-tropospheric EPV maximum (although, given the abundance of monsoon low-pressure systems in the Bay of Bengal, the climatological static stability profile may be influenced by moist convection in these disturbances).

In contrast, the quasi-geostrophic pseudopotential vorticity (QGPV) is obtained by a linear operation on ϕ' that does not allow the geostrophic relative vorticity (i.e. the first term on the right-hand side of Eq. (7)) to be multiplied by a vertically varying static stability. The contribution of static stability variations to the QGPV can be seen more clearly when the hydrostatic approximation and ideal gas law are used to express ϕ' in the last term in Eq. (7) in terms of an anomalous potential temperature, θ':

$$f_0 \frac{\partial}{\partial p}\left(\frac{1}{\sigma}\frac{\partial \phi'}{\partial p}\right) = f_0 \frac{\partial}{\partial p}\left(\frac{\theta'}{\frac{\mathrm{d}\overline{\theta}}{\mathrm{d}p}}\right). \tag{9}$$

Thus, vertical variations in static stability do contribute to the QGPV but are only scaled by f_0 and not by ζ.

Comparison of the three-dimensional fields of EPV and QGPV is complicated by the fact that QGPV is not simply an approximate form of EPV. The QGPV is conserved following the geostrophic wind on pressure surfaces and its inversion, while technically simple because of the linear form of Eq. (7), yields the geostrophic wind rather than the full wind. Nevertheless, the differences between QGPV and EPV fields, together with the large Rossby number, indicate that quasi-geostrophy likely provides a poor approximation to the full dynamics of MDs. In particular, quasi-geostrophy overemphasizes the importance of low-level dynamics and neglects the strong mid-tropospheric perturbations in MDs.

4. Results II: potential vorticity dynamics

4.1. *Adiabatic advection of mid-level potential vorticity*

We now turn to examination of the EPV field, since its relevance to storm motion is not subject to the requirement of low Rossby number. Furthermore, the EPV conservation equation lacks the non-advective source terms that exhibit a high degree of cancellation in the relative vorticity budget. Diabatic processes may complicate the EPV budget, but we will show that this is not of great importance for MD propagation.

The distributions of EPV and zonal wind u shown in Figure 1 for the July 1979 storm suggested that propagation might result from westward advection of the mid-tropospheric EPV maximum, a possibility that we now explore in detail. Instead of showing the climatological mean u centred on the composite mean storm, we define a temporally local time-mean flow by applying a 21 day running mean to the total u field. This was done because it is possible that subseasonal variability produces a mean flow for each depression that differs from the mean flow obtained using a calendar-based climatological average over many years. The storm-centred composite mean of this smoothed u is slightly more westward than the climatological mean u at the location of the peak EPV, but the difference is less than 1 m s^{-1} at most vertical levels (Figure 8(a), cf. black contours in Figure 3). This mean flow would advect the primary EPV maximum at 500 hPa to the west at a speed near 1 m s^{-1}, while advecting the lower tropospheric, secondary maximum to the east at about 2 m s^{-1}. This differential advection can also be inferred from a storm-centred composite of the climatological mean 500–700 hPa thickness, which shows a thickness gradient that is almost entirely meridional and thus a 500–700 hPa thermal wind that is almost entirely zonal (Figure 9, shading). The total u field is quite different from this mean flow (Figure 8(b)), indicating that nonlinear advection may be more important than advection by the mean flow. The total 500–700 hPa thermal wind is to the northwest at the storm centre, indicating that the net horizontal wind will advect the 500 hPa EPV northwest relative to the 700 hPa maximum (Figure 9, black contours). The Earth-relative net advective tendency of the entire EPV column is more difficult to infer, because the total u field shown in Figure 8(b) has such strong horizontal shears at the storm centre.

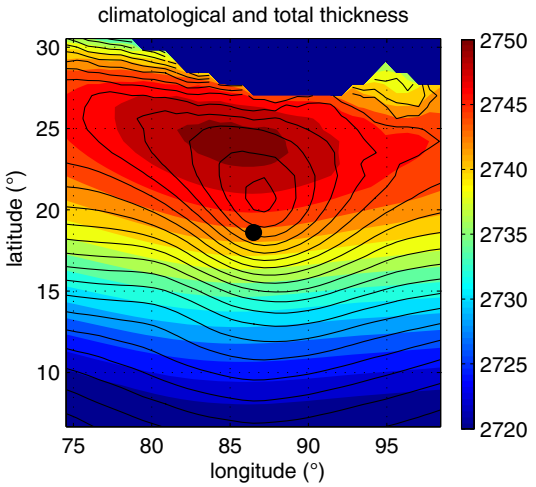

Figure 9. Climatological mean 500–700 hPa thickness (shading/colours) and total 500–700 hPa thickness (black contours), both composite means about the storm centre (denoted by the black dot). Both fields have contour intervals of 2 m and the dark (blue in online) region in the upper right is an area in which data have been masked out because the composite mean surface pressure is lower than 700 hPa.

Table 1. Mean values of the storm propagation velocities, total PV-weighted wind at the storm centre and the relevant 95% confidence interval for the mean, all in units of m s^{-1}.

	Zonal	Meridional
Observed motion	-1.5 ± 0.18	0.96 ± 0.11
500 hPa wind	-1.0 ± 0.20	1.8 ± 0.15
700 hPa wind	-0.64 ± 0.19	0.82 ± 0.13

In order to assess better the effect of horizontal advection on the primary EPV maximum, we compute the PV-weighted zonal and meridional wind, u_q and v_q, respectively:

$$u_q = \frac{1}{P}\iint_A uq\,\mathrm{d}A', \qquad v_q = \frac{1}{P}\iint_A vq\,\mathrm{d}A', \tag{10}$$

$$P = \iint_A q\,\mathrm{d}A', \tag{11}$$

where q is the EPV given by Eq. (2) and A is an area consisting of a $2^\circ \times 2^\circ$ box centred on the composite mean EPV maximum at 500 hPa (results were found to be insensitive to several changes in size of the averaging area). We evaluate u_q and v_q at 500 hPa for each six-hourly instance along the middle third of the track of every depression. We compare these values with the zonal and meridional components of the storm propagation velocity, defined as the time rate of change of the position of the 850 hPa vorticity maximum, as determined by the tracking algorithm. The mean storm propagation velocity is to the northwest at a total speed of 1.8 m s^{-1} and the mean PV-weighted wind at 500 hPa is of similar magnitude (2.1 m s^{-1}) but has a larger northward component (Table 1). Use of these mean values may be misleading, however, because the distributions of u_q and v_q at 500 hPa have relatively large standard deviations (3.4 and 2.1 m s^{-1}, respectively) and there is a similarly large spread in the components of the propagation velocity (Figure 10(a) and (d)).

The joint distribution of u_q and the zonal storm propagation velocity shows that the mode of the distribution lies on the 1:1 line at a westward speed of 2–3 m s^{-1} and the entire joint distribution tilts in the same direction as this 1:1 line (Figure 10(b)). The most frequently occurring relationship between 500 hPa winds and storm motion is thus consistent with simple adiabatic

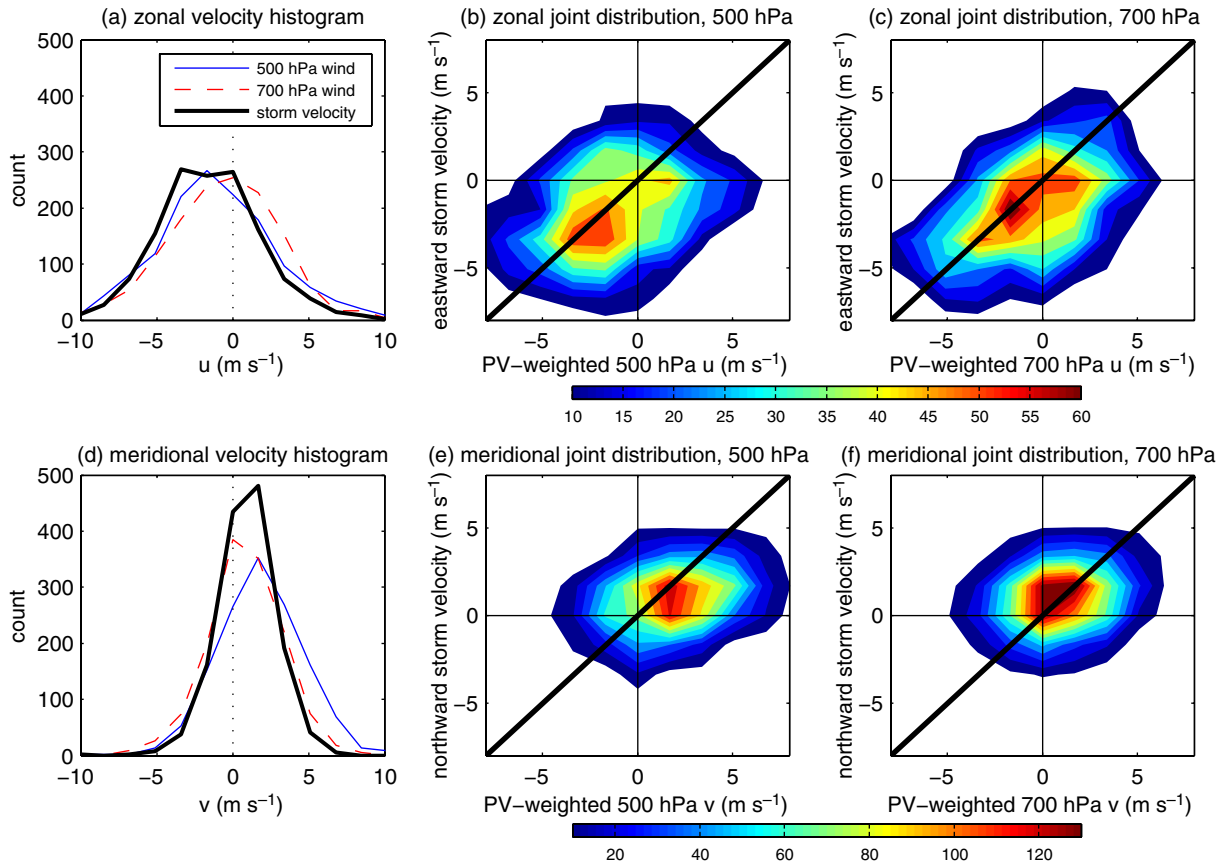

Figure 10. (a) Histogram of the EPV-weighted zonal wind at 500 hPa (thin line, blue in online) and 700 hPa (dashed line, red in online) and the zonal storm propagation velocity (thick black line); (d) shows the same quantities but in the meridional direction. (b) The joint distribution of zonal storm propagation velocity and the EPV-weighted zonal wind at 500 hPa, for every six-hourly sample along the middle third of each depression's track. The thick solid line is the 1:1 line; (c) shows the same quantities but at 700 hPa. (e) As in (b) but for the meridional storm propagation velocity and the EPV-weighted meridional wind at 500 hPa; (f) shows the same quantities but at 700 hPa. Shading/colours start at a count of 10 for all the joint distributions, with a contour interval of 5 for the distributions of zonal velocities and 10 for the meridional velocities, all with bin spacings of 1.7 m s^{-1}.

advection by the total zonal wind. The joint distribution of v_q and the meridional storm propagation velocity also has a mode very near the 1:1 line and is more sharply peaked than the joint distribution of zonal velocities (note the change in colour scale between Figure 10(b) and (e)). The joint distribution of meridional velocities does tilt away from the 1:1 line, indicating that meridional propagation for many storms is northward but at speeds slower than v_q.

To better understand the nature of the flow that might produce horizontal EPV advection, we inspect the stream function of the 500 hPa horizontal flow. In a fluid having a background poleward gradient of absolute vorticity, a cyclonic vortex will advect this background vorticity field to create a positive vorticity anomaly west of the vortex and a negative vorticity anomaly to the east. These induced anomalies are called beta gyres and their circulations constructively interfere to advect the initial vortex horizontally. This nonlinear self-advection has been well explored in the context of tropical cyclones (see review by Chan, 2005) and is often diagnosed by decomposition of the horizontal stream function into a component that is azimuthally symmetric about the vortex centre and an azimuthally asymmetric residual (e.g. Fiorino and Elsberry, 1989). Here, we separate the composite mean stream function of the horizontal wind at 500 hPa into a part that is symmetric about the 500 hPa EPV maximum and an asymmetric residual. The displacement of the stream function minimum from the EPV maximum is sufficiently large that northwestward advection of the EPV maximum is evident even in the total stream function (Figure 11(a)). The azimuthally asymmetric stream function shows a cyclonic gyre westsouthwest of the vortex centre and an anticyclonic gyre to the northeast that are consistent with a beta drift mechanism. The total 500 hPa wind is to the northwest, with a roughly 2 m s^{-1} magnitude, which is slightly stronger and in a more northward direction than the observed storm propagation velocity (cf. arrows in Figure 11(b), blue and red in the online version). The climatological mean wind has a much weaker magnitude that cannot account for the observed storm propagation (short arrow in Figure 11(b), green in the online version). All of this is consistent with the 500 hPa EPV maximum moving to the northwest by nonlinear self-advection, or beta drift.

4.2. *The trailing low-level vortex*

We now explore the mechanism responsible for propagation of the secondary, lower tropospheric EPV maximum, using several of the same analysis methods presented above. While the low-level EPV maximum is embedded in a layer of eastward time-mean flow, the total low-level flow is dominated by the vortex circulation so that the net low-level advection is also expected to be nonlinear (Figure 8). Indeed, the total horizontal stream function at 700 hPa is centred slightly southwest of the 700 hPa EPV maximum in the composite mean, as it was at 500 hPa, so that one would expect the low-level EPV maximum to be advected to the northwest by the total flow (Figure 12(a)). The net flow at the location of the EPV maximum is more clearly seen in the component of the 700 hPa stream function that is azimuthally asymmetric about the 700 hPa EPV maximum, which shows a cyclonic anomaly west of the EPV centre and an anticyclonic anomaly to the northeast (Figure 12(b)). This configuration is consistent with the northwestward total flow at the EPV maximum (the blue vector in the online version of the figure). In contrast, the climatological mean flow is stronger and directed almost due east (green vector in the online version; the red vector is the storm propagation velocity and is identical to the red vector in Figure 11(b)). Westerlies do exist in the total wind field at 700 hPa, but lie at least 500 km south of the vortex centre. These results show

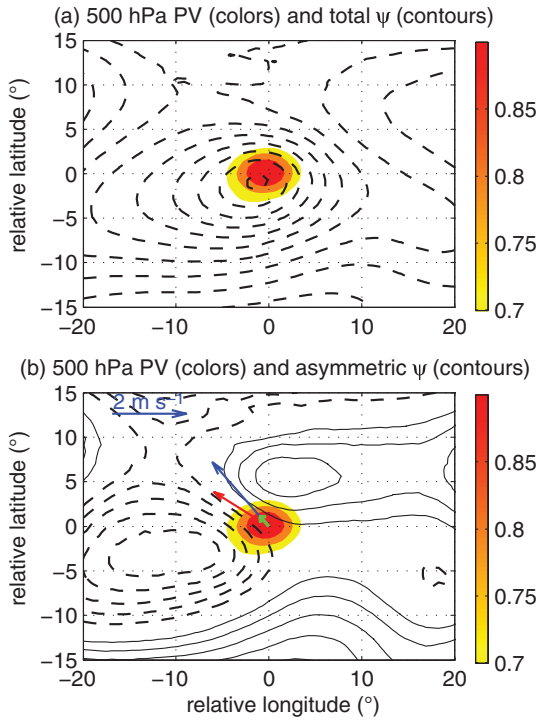

Figure 11. (a) Total horizontal stream function at 500 hPa (contours, dashed representing counterclockwise flow, with an interval of 10^6 m^2 s^{-1}) and 500 hPa EPV (shading/colours, interval 0.1 PVU starting at 0.7 PVU). (b) As in (a), but showing the azimuthally asymmetric part of the stream function, with a contour interval of 5×10^5 m^2 s^{-1}. The blue arrow (b) is the total horizontal wind vector averaged over a 2° × 2° box around the EPV maximum, the green arrow is the climatological mean horizontal wind vector averaged over the same area and the red arrow is the storm propagation velocity.

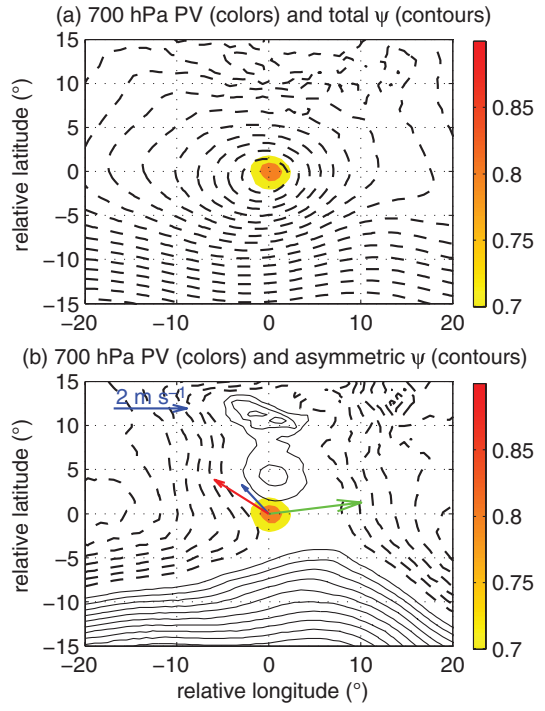

Figure 12. As in Figure 11, but at 700 hPa. The red vector is identical to the red vector in Figure 11.

that it is misleading to think of the low-level EPV maximum being advected to the east by the mean flow, because nonlinearities at that level are strong enough to reverse the direction of zonal advection.

Although the composite mean total wind at the 700 hPa EPV maximum is directed to the northwest, it is weaker than the observed storm propagation vector (magnitudes of 1.0 and 1.8 m s^{-1}, respectively) and is also weaker than the 500 hPa total wind at the location of the 500 hPa EPV maximum (Table 1, cf. blue vectors in the online versions of Figures 11(b) and 12(b) and total thickness contours in Figure 9). The distribution of 700 hPa PV-weighted zonal wind (u_q) is shifted to more eastward values compared with the zonal component of storm propagation (Figure 10(a)). However, the mode of the joint distribution of 700 hPa u_q and the zonal component of storm propagation lies on the 1:1 line (Figure 10(c)), indicating that zonal propagation can be explained by adiabatic advection alone for a large fraction of MDs. The composite mean behavior is altered by the fact that another subset of storms move westward relative to the total zonal flow, so that the joint distribution is skewed to the bottom right of Figure 10(c).

Finally, we ask whether horizontal advection of the low-level EPV maximum might arise in part from flow associated with the mid-level EPV maximum. The composite mean MD tilts to the southwest with height, so that the 500 hPa EPV maximum is centred about 100 km southwest of the 700 hPa maximum (Figure 13; note that the composite mean MD tilts northward with height between 850 and 700 hPa, so that the 850 hPa storm centre lies almost directly beneath the 500 hPa EPV maximum). The flow associated with an EPV feature extends vertically beyond the levels occupied by the feature and the vertical scale of that flow is given by the Rossby penetration depth:

$$H = \frac{fL}{N}, \tag{12}$$

where L is the horizontal scale of the feature and N is the buoyancy frequency. For the 500 hPa EPV maximum, $L \simeq 700$ km and $N \simeq 0.014\,\mathrm{s}^{-1}$, which gives a penetration depth of 2.3 km or about 170 hPa. Flow associated with the 500 hPa EPV maximum will thus make a negligible contribution to the surface wind, but is expected to be associated with a cyclonic component of the total 700 hPa flow. From the relative position of the two maxima shown in Figure 13, the 500 hPa EPV maximum is expected to advect the 700 hPa maximum to the northwest, in nearly the same direction as the total wind at the 700 hPa EPV centre (cf. Figure 12). Since the 700 hPa EPV maximum has a smaller horizontal scale as well as a weaker amplitude, its influence on the motion of the 500 hPa EPV field is expected to be much weaker. It may thus be misleading to think of horizontal advection of the low-level EPV maximum as being produced by a barotropic beta drift mechanism. Piecewise inversion of the EPV field (e.g. Davis and Emanuel, 1991) would allow the influence of one EPV anomaly on the other to be quantified, but inversion of the composite mean EPV structure is inappropriate because a nonlinear balance condition would be required for this high-Rossby-number flow. Inversion of the EPV field of individual storms is a relatively involved task that is left for future work.

4.3. *A case study of the potential vorticity budget*

Examination of the time evolution of EPV in storms with abundant precipitation would be incomplete without discussion of the tendencies due to diabatic processes. The ERA-Interim data do not include the diabatic heating rates needed to calculate those tendencies, so we turn to the ECMWF YOTC analysis, which does include diabatic heating rates, for analysis of a case study.
The EPV conservation equation is

$$\frac{\mathrm{D}q}{\mathrm{D}t} = \frac{1}{\rho}(\nabla \times \mathbf{F}) \cdot \nabla\theta + \frac{1}{\rho}\boldsymbol{\eta} \cdot \nabla\dot{\theta}, \tag{13}$$

where $\mathbf{F}$ is the mechanical forcing, $\mathrm{D}/\mathrm{D}t$ is the material derivative and $\dot{\theta}$ is $\mathrm{D}\theta/\mathrm{D}t$. We examine EPV tendencies above the planetary boundary layer and so neglect mechanical forcing, which allows the EPV budget to be rewritten as

$$\frac{\partial q}{\partial t} = \frac{1}{\rho}\boldsymbol{\eta} \cdot \nabla\dot{\theta} - \mathbf{u}_\mathrm{h} \cdot \nabla q - \omega\frac{\partial q}{\partial p}. \tag{14}$$

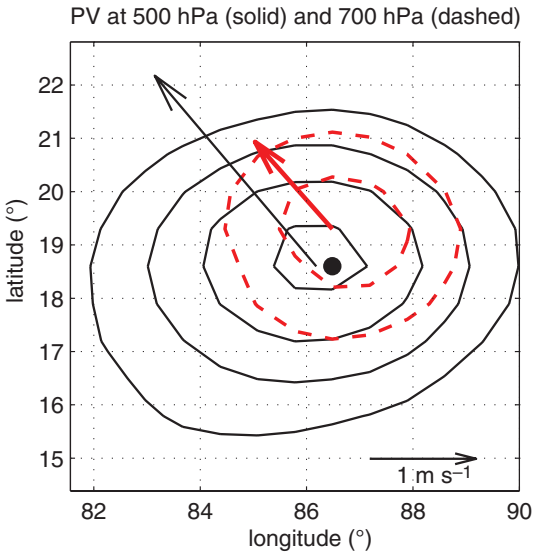

Figure 13. Composite mean Ertel's potential vorticity at 500 hPa (solid black contours) and 700 hPa (dashed contours, red in the online version). The contour interval is 0.1 PVU, starting at 0.7 PVU, for both levels. The total 500 hPa wind averaged over a 2° × 2° box centred on the 500 hPa EPV maximum is shown as the thin black vector and the total 700 hPa wind averaged over a 2° × 2° box centred on the 700 hPa EPV maximum is shown as the thick vector, red in the online version. The black dot indicates the position of the storm centre (i.e. the 850 hPa vorticity maximum).

The first term on the right-hand side of Eq. (14) is the EPV tendency due to diabatic processes, while the second and third terms are the tendencies due to horizontal and vertical advection, respectively.

Our track database contained nine MDs originating in the Bay of Bengal during the YOTC analysis period (May 2008–April 2010) and only four of these exhibited classic west-northwest propagation. The MD that formed on 12 September 2008 over the Bay of Bengal was chosen for this case study because of its longevity and roughly constant direction of propagation.

This MD traveled northwest toward the Indian subcontinent after its formation in the Bay of Bengal (Figure 14), producing copious precipitation in eastern and northern India. The anomalous stream function on 16 September 2008 depicts the cyclonic flow associated with the MD at 700 and 400 hPa. It briefly reached tropical storm status on 16 September 2008 (with a peak surface wind speed of 23 m s^{-1}) and was classified as 'Tropical Cyclone 02B' by the Joint Typhoon Warning Center (Cooper and Falvey, 2008).

Although September is late in the summer monsoon season, the climatological mean flow is still eastward at low levels and westward in the middle to upper troposphere (dashed contours in Figure 14(a) and (b), respectively) and the upper-level monsoon anticyclone is still strong (not shown). September 2008 was characterized by stronger low-level westerlies and weaker mid-level easterlies compared with the long-term climatological mean, so one would expect any eastward advection by the mean flow to be even stronger than usual. The convectively active centre of a Madden–Julian Oscillation (MJO) event was centred over the maritime continent, with amplitude 1.6 and phase 5 of the real-time, multivariate MJO index of Wheeler and Hendon (2004), as obtained from the Australian Bureau of Meteorology.* During boreal summer and fall, this phase of the MJO is typically associated with a northwest–southeast tilted band of active convection stretching from the Bay of Bengal to the western Pacific. The 30 day mean fields of precipitation and wind for September 2008 were consistent with this typical MJO structure, indicating that our example MD formed in the convectively active region of a boreal summer MJO event over the Bay of Bengal.

*http://cawcr.gov.au/staff/mwheeler/maproom/RMM/

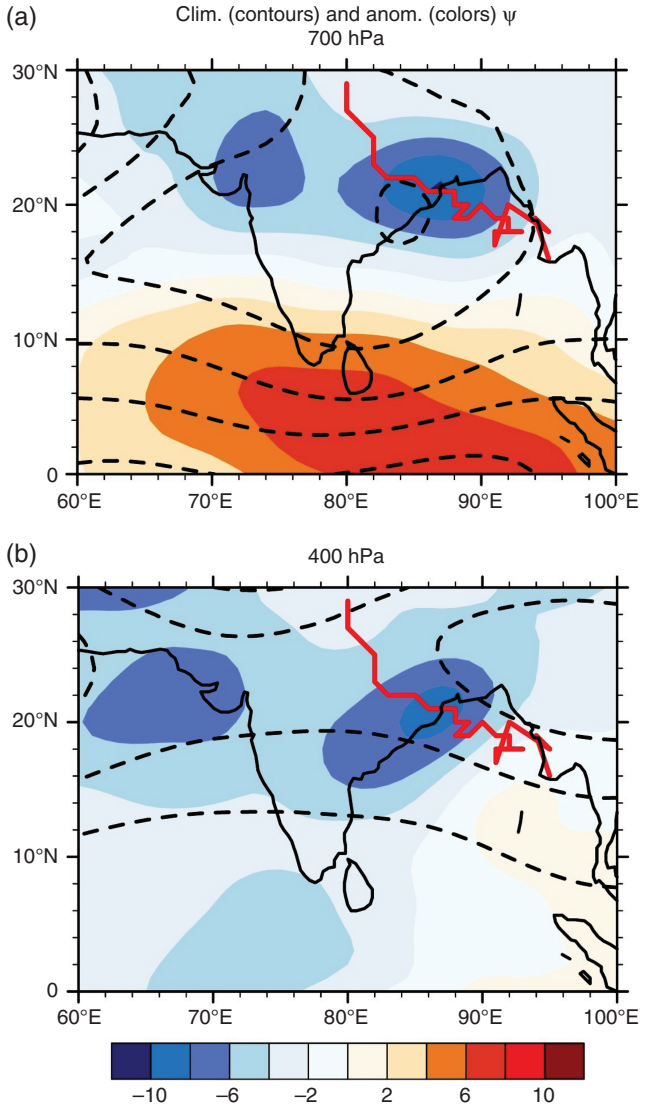

Figure 14. Horizontal stream function and storm track for the MD case study in September 2008. Shading/colours show the anomalous stream function (10^6 m^2 s^{-1}) at 1800 UTC on 16 September 2008. Black contours show the ERA-Interim climatological stream function during September (dashed negative, interval of 2 × 10^6 m^2 s^{-1}), corresponding to eastward flow over southern India in (a) and westward flow in (b). The thick line, red in the online version, depicts the track of the 500 hPa EPV maximum associated with the MD between 12 and 19 September 2008, subjectively identified from the YOTC data.

We calculated each term on the right-hand side of Eq. (14) for each six-hourly period, then averaged in time between September 14 and 18, relative to the location of the 500 hPa EPV maximum. The left-hand side of Eq. (14), which we refer to as the Eulerian EPV tendency, was calculated by centred differences in time at each spatial grid point and temporally averaged in a similar fashion. Finally, vertical averages were taken between 300 and 600 hPa, which is a layer that encompasses the composite mean midtropospheric EPV maximum (cf. Figure 8).

The Eulerian EPV tendency exhibits a dipole structure centred on the PV maximum, consistent with the observed propagation (Figure 15(a)). This storm's propagation was directed more to the west than the composite mean northwestward propagation discussed above, which is why the Eulerian tendency dipole points more toward the west. The horizontal advective tendency has a spatial structure and amplitude that is similar to the Eulerian tendency, while the diabatic and vertical advective tendencies are weaker and have structures that cannot account for the observed west-northwestward propagation. The diabatic tendency is produced almost entirely by the product of the vertical components of $\boldsymbol{\eta}$ and $\nabla\dot{\theta}$ (not shown) and there is some cancellation between the diabatic and vertical advective tendencies, as is common in convectively coupled tropical

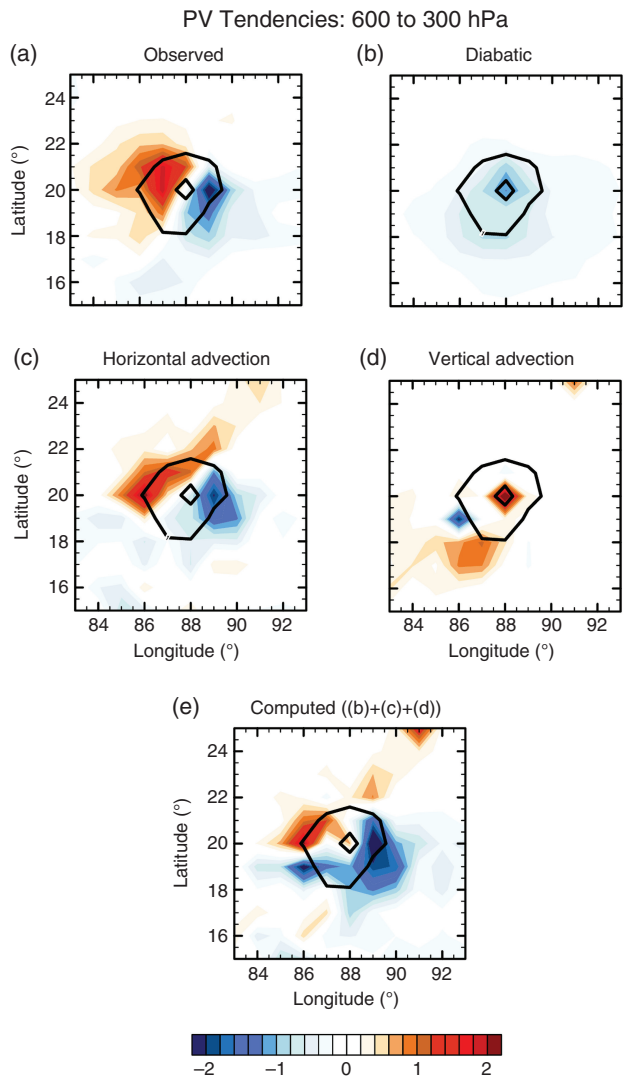

Figure 15. Time tendencies of EPV (shading/colors, in PVU day^{-1}) for the September 2008 MD. All quantities are averaged vertically between 600 and 300 hPa and temporally between September 15 and 18, centred on the storm centre. The EPV (black contours, 1.0 PVU interval) is shown for reference. (a) The Eulerian rate of change of EPV, (b) the diabatic EPV tendency, (c) the horizontal advective tendency, (d) the vertical advective tendency and (e) the sum of the diabatic and all advective tendencies.

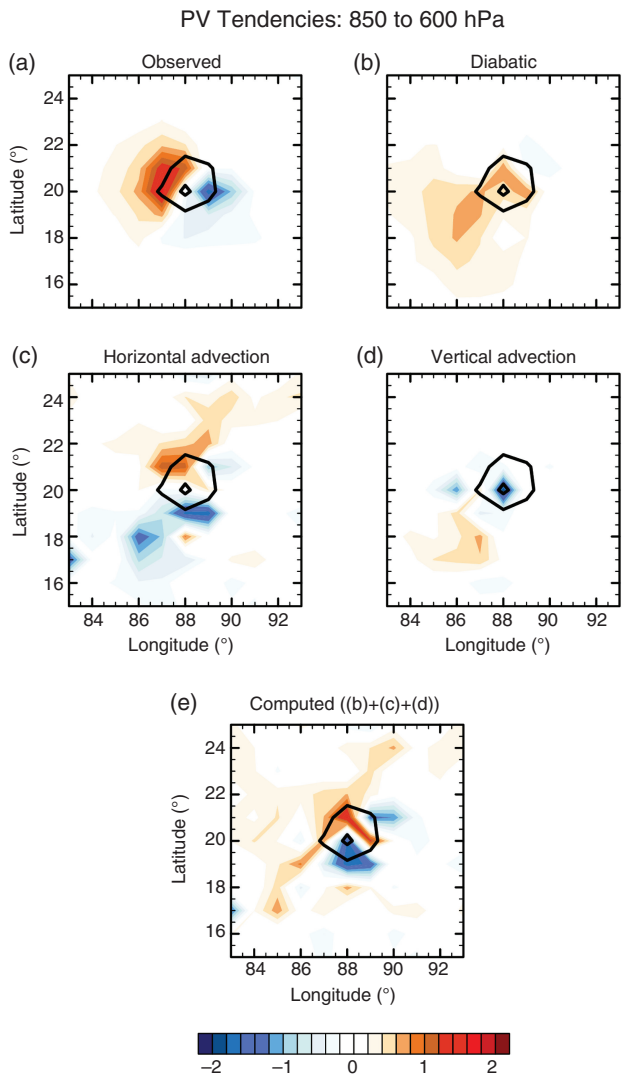

Figure 16. As in Figure 15, but averaged over a layer encompassing the secondary, lower tropospheric EPV maximum (600–850 hPa).

disturbances (e.g. Tory *et al.*, 2012). The sum of all terms on the right-hand side of Eq. (14) provides a decent match to the Eulerian tendency, although the negative part of the east–west dipole is more intense and horizontally extensive and the positive part is less extensive than in the Eulerian tendency. The primary EPV maximum of this MD clearly propagates westward because of adiabatic advection. This also shows that propagation of the 500 hPa PV maximum is not controlled by moist convective heating produced by low-level lifting. The motion of the primary EPV maximum is thus not slave to the low-level dynamics.

The analysis presented in the previous section indicated that adiabatic advection would produce westward motion of the 700 hPa PV maximum at a speed roughly half of that observed. This suggests that diabatic PV tendencies may be roughly as important as adiabatic beta drift for the motion of the secondary, low-level PV maximum. For the case of the September 2008 MD, the Eulerian EPV tendency averaged vertically from 600 to 850 hPa consists of a zonally oriented dipole that is consistent with the observed west-northwestward propagation (Figure 16). This matches the mid-level Eulerian EPV tendency presented above and confirms that there is little temporal change in the relative horizontal locations of the EPV maxima at 700 and 500 hPa. Horizontal advection moves the low-level EPV maximum of this MD toward the north-northwest. Diabatic and vertical advective tendencies combine to move the EPV maximum toward the southwest. The net computed tendency, i.e. the right-hand side of Eq. (14), does not have as clear a dipole structure as the Eulerian tendency, but is generally consistent with motion to the west-northwest. Although the EPV budget does not close as well in this lower tropospheric layer as it did in the middle troposphere, as might be expected due to mechanical boundary-layer processes, it is consistent with the hypothesis that diabatic heating modifies the motion of the low-level EPV anomaly. In other words, vertical advection and diabatic heating combine to shift the low-level EPV maximum to the southwest, while horizontal advection shifts it toward the north-northwest. The net motion of the low-level EPV maximum to the west-northwest is thus a superposition of these two effects.

The YOTC analysis period contained three other long-lived MDs that travelled to the west-northwest over the Indian subcontinent. Analysis of their EPV tendencies (not shown) reveals dynamics that are generally consistent with those of the case study just discussed. The Eulerian EPV tendency at upper levels (600–300 hPa) is largely explained by adiabatic horizontal advection for these other storms, although vertical advection also made a significant contribution for two storms. At lower levels (850–600 hPa), the westward propagation is due to a combination of northwestward horizontal advection and southwestward diabatic and vertical advective tendencies. This variability is consistent with the spread of the joint distributions shown in Figure 10: while the modes of these distributions lie on the 1:1 line, some storms did propagate westward slower or faster than the total zonal flow at the storm centre. Residuals in the EPV budgets of these three other MDs were generally at least as large as those shown here for the September 2008 case study.

5. Discussion and conclusions

Indian MDs have peak relative vorticity in the lower troposphere, where the time-mean wind is to the east. The northwestward propagation of these vortices thus appears to be upstream of the mean flow in which they are embedded and a series of articles written over several decades has attributed this motion to the low-level quasi-geostrophic lifting and associated vortex stretching that occurs downshear of the vortex centre (e.g. Rao and Rajamani, 1970; Sanders, 1984; Chen *et al.*, 2005). Here we have shown that important flaws exist in this explanation for the propagation of MDs. Firstly, vortex stretching would shift the vortex to the southwest, in a direction rotated 90° from the observed propagation vector. Secondly, lower tropospheric vortex stretching is nearly balanced by horizontal vorticity advection (and, in the planetary boundary layer, by a large budget residual that we attribute to dissipative processes) and so serves primarily to maintain the upright structure of the vortex rather than shift its position. The vorticity tendency needed to produce the observed northwest propagation cannot be primarily attributed to any single term in the lower tropospheric vorticity budget, indicating that the low-level vorticity budget may be a poor tool for understanding MD motion. The dynamical structure of MDs is confined to the lower troposphere only in the quasi-geostrophic limit and quasi-geostrophy is a poor approximation to the high-Rossby-number dynamics of these vortices.

We present the alternate hypothesis that Indian MDs are mid-tropospheric PV maxima that propagate by adiabatic beta drift. MDs are shown to consist of vertical PV columns that have peak amplitude in the middle troposphere (near 500 hPa) and weaker, secondary maxima near 700 hPa. Although previous studies of low-level, quasi-geostrophic dynamics emphasized the need to overcome eastward advection by the time-mean flow, we find that the total horizontal flow in MDs is large compared with the time-mean flow, so that horizontal advection is highly nonlinear. This was seen when comparing the total zonal wind with the time-mean zonal wind in storm-centred composites (Figure 8) and when comparing the climatological mean horizontal flow with the total horizontal flow for a case study (Figure 14). The total wind at the location of the mid-tropospheric PV maximum is directed to the northwest and has a similar direction and magnitude to the observed storm propagation velocity; covariance between the zonal storm propagation velocity and the zonal wind at the PV maximum also supports the hypothesis that propagation is caused by adiabatic PV advection. The total wind at the PV maximum is directed further north than the storm propagation velocity and we suggest that the PV tendency produced by convectively coupled ascent southwest of the vortex centre adds to the horizontal advective tendencies to produce the observed propagation. Similar arguments hold for the secondary PV maximum in the lower troposphere. Diabatic and vertical advective PV tendencies may play a more important role in the movement of the lower tropospheric PV maximum, but total horizontal advection at those levels is still nonlinear and to the northwest. These roles for adiabatic horizontal advection and diabatic processes were supported by analysis of the EPV budget in a case study.

Nonlinear horizontal advection of PV at a given vertical level can be produced by flow associated with a high-amplitude PV anomaly at the same level (e.g. beta drift) or by flow associated with a PV anomaly at a different vertical level. The southwestward tilt with height of the composite mean PV column suggests that the 500 hPa PV maximum propagates to the west by beta drift, while at least part of the horizontal advection of the 700 hPa PV maximum is accomplished by flow associated with the 500 hPa PV maximum. The horizontal scale of the 500 hPa PV maximum is large enough and the thermal stratification is small enough to permit such vertical interaction; the fact that the low-level PV maximum is located northeast of the mid-level maximum is consistent with the former being advected to the northwest by flow associated with the latter. In contrast, flow attributed to the low-level PV maximum would advect the mid-level PV maximum to the southeast and so cannot explain the observed propagation to the northwest. A quantitative estimate of vertical interaction between the mid- and low-level PV maxima would require piecewise inversion of the PV field of individual MD cases and is a task left for future work.

It is entirely possible that mean flow advection could add to beta drift to alter the net storm propagation velocity of MDs, as it commonly does for tropical cyclones (e.g. Chan, 2005). Mean flow advection did not seem to affect propagation of the composite mean MD greatly because its EPV maximum was positioned so close to the line of zero zonal wind, but the distance of storms from the zero zonal wind line varied across the ensemble of MDs and throughout the lifetime of individual MDs. We speculate that MDs propagate to the north-northeast over both northern India and the southern Bay of Bengal (Figure 2) because the 500 hPa mean flow in this region consists of stronger mean westerlies that add to the motion induced by beta drift. We do not know why the composite mean MD lies so close to the line of zero zonal wind, but Australian tropical cyclogenesis also tends to occur near the line of zero zonal wind (McBride and Keenan, 1982). This may be a preferred location for MD spin-up simply because it is a region of high ambient vorticity associated with horizontal shear. We are exploring the statistical associations between MD genesis and the climatological mean state in a separate work.

Although there are some open questions regarding the dynamics involved in the adiabatic, nonlinear advection responsible for MD propagation, the propagation clearly results from a mechanism distinct from the previous idea of low-level, quasi-geostrophic vortex stretching. Quasi-geostrophic lifting does occur and seems to explain why precipitating ascent is located southwest of the vorticity maximum, but the associated vorticity and diabatic PV tendencies make a seemingly minor contribution to the net storm propagation. Furthermore, a quantitative theory for the distribution of MD ascent that incorporates the diabatic effects of moist convection has yet to be presented, so the quasi-geostrophic omega equation cannot even be regarded as providing a closed theory for the spatial structure of MDs.

It may seem surprising that PV is a conceptually useful quantity in the study of MDs, because the abundant precipitation in tropical systems can produce diabatic tendencies that dominate the evolution of the PV field. However, these diabatic tendencies in MDs are substantially smaller than the horizontal advective tendencies and clearly do not resemble the Eulerian tendencies needed to reproduce the observed storm motion. This fact alone confirms that the propagation of the mid-tropospheric PV maximum cannot be regarded as being controlled by low-level lifting and any associated diabatic PV tendencies and suggests that MD propagation can indeed be viewed in terms of the dynamics of the mid-tropospheric PV maximum. This adiabatic view of MD dynamics will be inadequate for explaining the growth in amplitude of the initial PV anomaly, because diabatic processes are needed to create the localized, high-amplitude PV maxima of mature MDs. However, it provides one useful application of traditional, dry PV thinking to tropical dynamics and constitutes part of what may be a new dynamical paradigm for these important vortices.

Acknowledgements

This work was supported by Office of Naval Research Young Investigator Program award N00014-11-1-0617 and National Science Foundation award AGS-1253222. WRB acknowledges helpful conversations with Brian Mapes, who independently and concurrently recognized that the propagation of Indian MDs might be controlled by the evolution of mid-tropospheric PV maxima. ERA-Interim data were accessed in November 2011 from the Research Data Archive at the National Center for Atmospheric Research, Computational and Information Systems Laboratory, Boulder, CO (http://rda.ucar.edu/datasets/ds627.0). ECMWF–YOTC data were accessed

in August 2013 from the ECMWF Data Server, Reading, UK (http://apps.ecmwf.int/datasets/data/yotc_od/).

References

Ajayamohan R, Merryfield W, Kharin V. 2010. Increasing trend of synoptic activity and its relationship with extreme rain events over central India. *J. Clim.* **23**: 1004–1013.

Beattie JC, Elsberry RL. 2012. Western North Pacific monsoon depression formation. *Weather and Forecasting* **27**: 1413–1432.

Beattie JC, Elsberry RL. 2013. Horizontal structure of monsoon depressions in the western North Pacific at formation time. *Geophys. Res. Lett.* **40**: 983–987, doi: 10.1002/grl.50198.

Berry GJ, Reeder MJ, Jakob C. 2012. Coherent synoptic disturbances in the Australian monsoon. *J. Clim.* **25**: 8409–8421.

Bluestein HB. 1992. *Synoptic–Dynamic Meteorology in Midlatitudes*, Vol. 1: Principles of Kinematics and Dynamics. Oxford University Press: New York, NY.

Chan J. 2005. The physics of tropical cyclone motion. *Annu. Rev. Fluid Mech.* **37**: 99–128.

Charney J, Stern M. 1962. On the stability of internal baroclinic jets in a rotating atmosphere. *J. Atmos. Sci.* **19**: 159–172.

Chatterjee P, Goswami BN. 2004. Structure, genesis and scale selection of the tropical quasi-biweekly mode. *Q. J. R. Meteorol. Soc.* **130**: 1171–1194.

Chen T, Weng S. 1999. Interannual and intraseasonal variations in monsoon depressions and their westward-propagating predecessors. *Mon. Weather Rev.* **127**: 1005–1020.

Chen T, Yoon J, Wang S. 2005. Westward propagation of the Indian monsoon depression. *Tellus A* **57**: 758–769.

Cooper G, Falvey RJ. 2008. 'Annual tropical cyclone report, 2008', Technical report. US Naval Maritime Forecast Center/Joint Typhoon Warning Center: Pearl Harbor, HI, 116 pp.

Daggupaty S, Sikka D. 1977. On the vorticity budget and vertical velocity distribution associated with the life cycle of a monsoon depression. *J. Atmos. Sci.* **34**: 773–792.

Davidson N, Holland G. 1987. A diagnostic analysis of two intense monsoon depressions over Australia. *Mon. Weather Rev.* **115**: 380–392.

Davies-Jones R. 1991. The frontogenetical forcing of secondary circulations. Part I: The duality and generalization of the Q vector. *J. Atmos. Sci.* **48**: 497–509.

Davis CA. 1992. Piecewise potential vorticity inversion. *J. Atmos. Sci.* **49**: 1397–1411.

Davis CA, Emanuel KA. 1991. Potential vorticity diagnostics of cyclogenesis. *Mon. Weather Rev.* **119**: 1929–1953.

Dee D, Uppala S, Simmons A, Berrisford P, Poli P, Kobayashi S, Andrae U, Balmaseda M, Balsamo G, Bauer P, Bechtold P, Beljaars ACM, van de Berg L, Bidlot J, Bormann N, Delsol C, Dragani R, Fuentes M, Geer AJ, Haimberger L, Healy SB, Hersbach H, Hólm EV, Isaksen L, Kållberg P, Köhler M, Matricardi M, McNally AP, Monge-Sanz BM, Morcrette J-J, Park B-K, Peubey C, de Rosnay P, Tavolato C, Thépaut J-N, Vitart F. 2011. The ERA-Interim reanalysis: Configuration and performance of the data assimilation system. *Q. J. R. Meteorol. Soc.* **137**: 553–597, doi: 10.1002/qj.828.

Emanuel KA, Neelin JD, Bretherton CS. 1994. On large-scale circulations in convecting atmospheres. *Q. J. R. Meteorol. Soc.* **120**: 1111–1143.

Ertel H. 1942. Ein neuer hydrodynamischer Wirbelsatz. *Meteorol. Z.* **59**: 277–281.

Fiorino M, Elsberry R. 1989. Some aspects of vortex structure related to tropical cyclone motion. *J. Atmos. Sci.* **46**: 975–990.

Godbole R. 1977. The composite structure of the monsoon depression. *Tellus* **29**: 25–40.

Goswami B. 1987. A mechanism for the west-north-west movement of monsoon depressions. *Nature* **326**: 376–378.

Hakim GJ, Keyser D, Bosart LF. 1996. The Ohio Valley wave-merger cyclogenesis event of 25–26 January 1978. Part II: Diagnosis using quasi-geostrophic potential vorticity inversion. *Mon. Weather Rev.* **124**: 2176–2205.

Haynes P, McIntyre M. 1987. On the evolution of vorticity and potential vorticity in the presence of diabatic heating and frictional or other forces. *J. Atmos. Sci.* **44**: 828–841.

Hodges K. 1995. Feature tracking on the unit sphere. *Mon. Weather Rev.* **123**: 3458–3465.

Hodges K. 1998. Feature-point detection using distance transforms: Application to tracking tropical convective complexes. *Mon. Weather Rev.* **126**: 785–795.

Hoskins B, Draghici I, Davies H. 1978. A new look at the ω-equation. *Q. J. R. Meteorol. Soc.* **104**: 31–38.

Hoskins B, McIntyre M, Robertson A. 1985. On the use and significance of isentropic potential vorticity maps. *Q. J. R. Meteorol. Soc.* **111**: 877–946.

Hurley JV, Boos WR. 2014. A global climatology of monsoon low-pressure systems. *Q. J. R. Meteorol. Soc.*, doi: 10.1002/qj.2447.

Jones SC. 1995. The evolution of vortices in vertical shear. I: Initially barotropic vortices. *Q. J. R. Meteorol. Soc.* **121**: 821–851.

Keshavamurty R, Asnani G, Pillai P, Das S. 1978. Some studies of the growth of monsoon disturbances. *Proc. Indian Acad. Sci., Sect. A: Earth Planet. Sci.* **87**: 61–75.

Kiladis GN, Thorncroft CD, Hall NM. 2006. Three-dimensional structure and dynamics of African easterly waves. Part I: Observations. *J. Atmos. Sci.* **63**: 2212–2230.

Krishnamurthy V, Ajayamohan R. 2010. Composite structure of monsoon low-pressure systems and its relation to Indian rainfall. *J. Clim.* **23**: 4285–4305.

Krishnamurti TN, Kanamitsu M, Godbole R, Chang C, Carr F, Chow JH. 1975. Study of a monsoon depression (I): Synoptic structure. *J. Meteorol. Soc. Jpn.* **53**: 227–240.

Krishnamurti TN, Molinari J, lu Pan H, Wong V. 1977. Downstream amplification and formation of monsoon disturbances. *Mon. Weather Rev.* **105**: 1281–1297.

McBride J, Keenan T. 1982. Climatology of tropical cyclone genesis in the Australian region. *J. Climatol.* **2**: 13–33.

Moncrieff MW, Waliser DE, Miller MJ, Shapiro MA, Asrar GR, Caughey J. 2012. Multiscale convective organization and the YOTC virtual global field campaign. *Bull. Am. Meteorol. Soc.* **93**: 1171–1187.

Montgomery MT, Farrell BF. 1991. Moist surface frontogenesis associated with interior potential vorticity anomalies in a semigeostrophic model. *J. Atmos. Sci.* **48**: 343–368.

Montgomery MT, Farrell BF. 1992. Polar low dynamics. *J. Atmos. Sci.* **49**: 2484–2505.

Mooley DA, Shukla J. 1987. 'Characteristics of the westward-moving summer monsoon low-pressure systems over the Indian region and their relationship with the monsoon rainfall', Technical Report. University of Maryland Center for Ocean–Land–Atmosphere Interactions: College Park, MD, 218 pp.

Moore RW, Montgomery MT. 2004. Reexamining the dynamics of short-scale, diabatic Rossby waves and their role in midlatitude moist cyclogenesis. *J. Atmos. Sci.* **61**: 754–768.

Moore RW, Montgomery MT. 2005. Analysis of an idealized, three-dimensional diabatic Rossby vortex: A coherent structure of the moist baroclinic atmosphere. *J. Atmos. Sci.* **62**: 2703–2725.

Parker DJ, Thorpe AJ. 1995. Conditional convective heating in a baroclinic atmosphere: A model of convective frontogenesis. *J. Atmos. Sci.* **52**: 1699–1711.

Rao K, Rajamani S. 1970. Diagnostic study of a monsoon depression by geostrophic baroclinic model. *Indian J. Meteorol. Geophys.* **21**: 187–194.

Raymond D, Jiang H. 1990. A theory for long-lived mesoscale convective systems. *J. Atmos. Sci.* **47**: 3067–3077.

Reasor PD. 2001. Three-dimensional alignment and corotation of weak, TC-like vortices via linear vortex Rossby waves. *J. Atmos. Sci.* **58**: 2306–2330.

Reasor PD, Montgomery MT, Grasso LD. 2004. A new look at the problem of tropical cyclones in vertical shear flow: Vortex resiliency. *J. Atmos. Sci.* **61**: 3–22.

Rossby CG. 1940. Planetary flow patterns in the atmosphere. *Q. J. R. Meteorol. Soc.* **66**: 68–87.

Saha K, Chang C. 1983. The baroclinic processes of monsoon depressions. *Mon. Weather Rev.* **111**: 1506–1514.

Saha K, Sanders F, Shukla J. 1981. Westward propagating predecessors of monsoon depressions. *Mon. Weather Rev.* **109**: 330–343.

Sanders F. 1984. Quasi-geostrophic diagnosis of the monsoon depression of 5–8 July 1979. *J. Atmos. Sci.* **41**: 538–552.

Sikka D. 1977. Some aspects of the life history, structure and movement of monsoon depressions. *Pure Appl. Geophys.* **115**: 1501–1529.

Sikka DR. 2006. 'A study on the monsoon low-pressure systems over the Indian region and their relationship with drought and excess monsoon seasonal rainfall', COLA Technical Report 217. Center for Ocean–Land–Atmosphere Studies: Calverton, MD, 145 pp.

Snyder C, Lindzen RS. 1991. Quasi-geostrophic wave–CISK in an unbounded baroclinic shear. *J. Atmos. Sci.* **48**: 76–86.

Sobel AH, Horinouchi T. 2000. On the dynamics of easterly waves, monsoon depressions, and tropical depression type disturbances. *J. Meteorol. Soc. Jpn.* **78**: 167–173.

Sutcliffe R. 1947. A contribution to the problem of development. *Q. J. R. Meteorol. Soc.* **73**: 370–383.

Tory KJ, Kepert J, Sippel J, Nguyen C. 2012. On the use of potential vorticity tendency equations for diagnosing atmospheric dynamics in numerical models. *J. Atmos. Sci.* **69**: 942–960.

Trenberth KE. 1978. On the interpretation of the diagnostic quasi-geostrophic omega equation. *Mon. Weather Rev.* **106**: 131–137.

Wang Y, Holland G. 1996. The beta drift of baroclinic vortices. Part I: Adiabatic vortices. *J. Atmos. Sci.* **53**: 411–427.

Wang B, Elsberry RL, Yuqing W, Liguang W. 1999. Dynamics in tropical cyclone motion: A review. *Chin. J. Atmos. Sci.* **22**: 416–434.

Wheeler M, Hendon H. 2004. An all-season real-time multivariate MJO index: Development of an index for monitoring and prediction. *Mon. Weather Rev.* **132**: 1917–1932.

Yoon J, Chen T. 2005. Water vapor budget of the Indian monsoon depression. *Tellus A* **57**: 770–782.

Yoon JH, Huang WRJ. 2012. Indian monsoon depression: Climatology and variability. In *Modern Climatology*, Chapter 2, Wang SY. (ed.): 45–72. InTech: Rijeka, Croatia.

